Clinical Imaging 39 (2015) 809–814

Contents lists available at ScienceDirect

Clinical Imaging

journal homepage: http://www.clinicalimaging.org

Myocardial signal density levels and beam-hardening artifact attenuation using dual-energy computed tomography☆

Gaston A. Rodriguez-Granillo [a,*], Patricia Carrascosa [a], Silvina Cipriano [a], Macarena de Zan [a], Alejandro Deviggiano [a], Carlos Capunay [a], Ricardo C. Cury [b]

[a] Department of Cardiovascular Imaging, Diagnóstico Maipú, Buenos Aires, Argentina
[b] Miami Cardiac and Vascular Institute and Baptist Health of South Florida, Miami, FL, United States

ARTICLE INFO

Article history:
Received 19 February 2015
Received in revised form 30 March 2015
Accepted 8 April 2015

Keywords:
Myocardial perfusion
Perfusion defect
Myocardial infarction
Ischemia
Computed tomography

ABSTRACT

The assessment of myocardial perfusion using single-energy (SE) imaging is influenced by beam-hardening artifacts (BHA). We sought to explore the ability of dual-energy (DE) imaging to attenuate the presence of BHA. Myocardial signal density (SD) was evaluated in 2240 myocardial segments (112 for each energy level) and in 320 American Heart Association segments among the SE group. Compared to DE reconstructions at the best energy level, SE acquisitions showed no significant differences overall regarding myocardial SD or signal-to-noise ratio. The segments most commonly affected by BHA showed significantly lower myocardial SD at the lowest energy levels, progressively normalizing at higher energy levels.

1. Introduction

The evaluation of myocardial perfusion imaging by means of multidetector computed tomography (CT) has earned interest during the past decade and shows promise to provide a significant incremental value over coronary computed tomography angiography (CCTA) [1–5]. The growing need to assess the physiological impact of a given atherosclerotic lesion is supported by the relatively poor relationship between the degree of stenosis and the presence of ischemia [6,7].

Several ex vivo and in vivo studies provide a robust proof of concept, with a close correlation between contrast kinetics of gadolinium-based agents in magnetic resonance imaging and iodinated contrast agents in CT [8,9]. Myocardial CT perfusion (CTP) has been validated in a number of clinical scenarios, including the evaluation of patients with low to intermediate likelihood of coronary artery disease (CAD), as well as for the triage of patients with acute chest pain [3,4,9].

Notwithstanding, the assessment of CTP using conventional single-energy (SE) acquisitions is influenced by the presence of beam-hardening artifacts (BHA) [10,11]. These artifacts are related to the polychromatic nature of X-rays and to the energy-dependency of X-ray attenuation, and lead to a significant drop in attenuation levels in areas adjacent to highly enhanced structures, commonly resembling perfusion defects in certain left ventricular segments during CCTA [11]. Dual-energy (DE) CT imaging appears as an intriguing technique for CTP, mainly driven by its ability to obtain synthesized monochromatic image reconstructions that might attenuate some of the aforementioned technical issues [5,12]. We therefore sought to explore the ability of DE CTP to mitigate the presence of BHA.

2. Materials and methods

The present study was a single-center, investigator-driven, observational study that involved consecutive patients without a history of CAD who were referred for CCTA evaluation at our institution due to atypical chest pain and evidence of a normal stress-rest single-photon emission CT within the previous 3 months. All patients included were >18 years old; in sinus rhythm; able to maintain a breath-hold for ≥15 s; and without a history of contrast-related allergy, renal failure, or hemodynamic instability. Additional exclusion criteria comprised a body mass index >32 kg/m^2 or a history of previous myocardial infarction, percutaneous or surgical coronary revascularization, severe valve disease, chronic heart failure, chronic obstructive pulmonary disease, or high-degree atrioventricular block. Patients with diabetes, left ventricular hypertrophy, and obstructive (≥50% stenosis) atherosclerotic coronary lesions were also excluded. In addition, patients with intrascan mild heart rhythm abnormalities leading to motion artifacts such as premature

Abbreviations: SE, single energy; DE, dual energy; CTP, computed tomography perfusion; SD, signal density; BHA, beam-hardening artifacts; CCTA, coronary computed tomography angiography; CAD, coronary artery disease.

☆ We declare that Drs. Patricia Carrascosa and Ricardo C. Cury provided consultant work for GE Healthcare in the past 12 months. There are no competing interests related to the manuscript for any of the other authors.

* Corresponding author. Av Maipú 1668, Vicente López (B1602ABQ), Buenos Aires, Argentina. Tel./fax: +54 11 48377596.
E-mail address: grodriguezgranillo@gmail.com (G.A. Rodriguez-Granillo).

http://dx.doi.org/10.1016/j.clinimag.2015.04.007
0899-7071/

beats and heart rate <40 bpm were excluded. Two cohorts of patients were sequentially included. The study group was acquired using DE scan; and the control group, using conventional SE scan.

3. Image acquisition

Patients with a heart rate of more than 65 bpm received 50 mg metoprolol orally or 5 mg intravenous propralonol if needed in order to achieve a target heart rate of less than 60 bpm.

Patients were scanned using a DE scanner equipped with gemstone detectors with fast primary speed and low afterglow designed for spectral imaging (Discovery HD 750; GE Medical Systems, Milwaukee, WI, USA). All scans were performed using prospective electrocardiogram gating using a 100-ms padding centered at 75% of the cardiac cycle. Other scanner-related parameters were a collimation width of 0.625 mm and a slice interval of 0.625 mm. Maximum tube voltage and current of SE scans were adjusted according to the body habitus (100 kV or 120 kV for patients with body mass index <30 kg/m^2 or larger, respectively).

DE imaging was performed by rapid switching (0.3–0.5 ms) between low and high tube potentials (80–140 kV) from a single source, thereby allowing the reconstruction of low- and high-energy projections and generation of monochromatic image reconstructions with 10-keV increments from 40 to 140 keV. Iterative reconstruction was performed in all cases at 40% adaptive statistical iterative reconstruction. For DE acquisitions, 60 keV is so far the lowest monoenergetic level available for the reconstruction of images utilizing an iterative reconstruction algorithm. A dual-phase protocol with 50–70 ml of iodinated contrast (iobitridol; Xenetix 350, Guerbet, France) followed by a 30–40-ml saline flush was injected through an arm vein. A bolus tracking technique was used to synchronize the arrival of contrast at the level of the coronary arteries with the start of the scan. Image acquisition was performed after sublingual administration of 2.5–5 mg of isosorbide dinitrate.

The institution's Ethics Committee approved the study protocol, which complied with the Declaration of Helsinki, and written informed consent was obtained from all patients.

4. Myocardial perfusion analysis

CCTA image analysis was performed off-line on a dedicated workstation using a commercially available dedicated software tool (AW 4.6; GE Healthcare). Two experienced observers (PC, GRG) were randomly assigned to independently analyze patients of either of the two groups. CT images were analyzed at mid diastole using a smooth filter in axial planes and multiplanar reconstructions. Short-axis views were obtained initially using 5-mm average multiplanar reconstructions from base to apex, with the full dataset available for the reader. Using standardized regions of interest of 10 to 20 mm^2, myocardial signal density (SD) and noise (standard deviation of myocardial SD) were determined for every segment according to the American Heart Association (AHA) 17-segment myocardial model [13]. AHA segment 17 corresponding to the left ventricular apex was excluded from the analysis since it encompasses a thin myocardial wall and is therefore prone to measurement error. Left ventricular and right ventricular chamber mean SDs were evaluated at basal, mid, and apical short axis.

Measurements among the DE group were performed at different energy levels ranging from 40 to 100 keV. SD ratio, which is highly related to myocardial blood flow measured by microspheres, was determined as previously described: myocardial SD/left ventricular blood pool SD (at the corresponding level; basal, mid, or apical) [14]. Myocardial SD, SD ratio, and signal-to-noise ratio were evaluated at every AHA segment.

CT effective radiation dose was derived by multiplying the dose–length product with the weighting (k) value of 0.014 mSv/mGy/cm for chest examinations, as suggested by the Society of Cardiovascular Computed Tomography [15].

5. Statistical analysis

Discrete variables are presented as counts and percentages; and continuous variables, as mean±standard deviation. Comparisons among groups were performed using paired-samples t test, independent-samples t test, analysis of variance (ANOVA), χ^2 tests, or Fisher's Exact Tests, as indicated. Post hoc comparisons were explored using least significant difference tests. We explored correlations between the basal inferolateral (BIL) segment SD, previously established as the most common location of BHA [11], and variables thought to be related to the presence of BHA using Spearman correlation coefficients. The agreement between observers for the identification of BHA was assessed using the Kappa coefficient. A two-sided P value of less than .05 indicated statistical significance. Statistical analyses were performed with use of SPSS software, version 22 (Chicago, IL, USA).

6. Results

Forty patients constituted the study population (DE group, $n=20$; SE group, $n=20$). The mean age was 59.6±12.0 years, and 28 (70%) were male. Demographical characteristics were similar between groups, as well as the heart rate and the effective radiation dose (Table 1).

Myocardial SD levels were evaluated in 2240 AHA myocardial segments (112 for each energy level from 40 to 100 keV at 10-keV intervals) among the DE group and in 320 AHA segments in the SE group.

7. Myocardial SD levels using DE and SE imaging

Among the DE group, myocardial SD levels and myocardial SD ratio were higher at low energy levels, with significantly lower SD levels at increasing energy levels (Tables 2 and 3, and Figs. 1 and 3). In turn, myocardial signal-to-noise ratio was not significantly influenced by the energy level applied, although 70 keV was identified as the energy level with the best overall signal-to-noise ratio (Table 4). Compared to DE reconstructions at 70 keV, SE acquisitions showed no significant differences overall regarding myocardial SD levels or signal-to-noise ratio, whereas a number of segments showed lower SD ratio among the SE group (Fig. 2).

8. Effect on BHA

Among the SE group, a total of 35/320 segments (10.9%) were identified as BHA by both observers (kappa 0.82; $P<.0001$), whereas among the DE group, a total of 42/320 segments (13.1%) were identified as BHA by both observers (kappa 0.83; $P<.0001$).

On a per-patient level, 18 (90%) patients among the SE group showed at least one segment with BHA, most commonly located at the BIL (65%)

Table 1
Demographical characteristics

	DE ($n=20$)	SE ($n=20$)	P
Age (years±S.D.)	60.8±9.9	58.5±14.3	.56
Male, n (%)	12 (60%)	16 (80%)	.30
Hypertension, n (%)	12 (60%)	10 (50%)	.75
Hypercholesterolemia, n (%)	11 (55%)	10 (50%)	.99
Previous smoking, n (%)	7 (35%)	2 (10%)	.13
Body mass index (kg/m^2±S.D.)	27.9±3.2	27.8±3.9	.88
Heart rate (bpm±S.D.)	63.3±5.8	63.1±5.4	.93
Effective dose (mSv±S.D.)	3.1±0.4	3.3±0.7	.34

Comparisons performed using Fisher's Exact Test.

Table 2
Myocardial SD (Hounsfield units, HU) of left ventricular segments (AHA segmentation) among different energy levels using DE acquisitions

	SE	40 keV	50 keV	60 keV	70 keV	80 keV	90 keV	100 keV	*P* (ANOVA)
AHA-1	78.3±12.9	197.0±73.7	136.7±43.3	100.0±31.4	79.2±25.2	65.7±17.0	57.4±13.7	51.1±12.0	<.0001
AHA-2	90.6±27.8	267.6±79.3	183.0±52.3	133.0±34.0	101.4±23.3	81.4±16.6	67.8±12.6	57.7±10.1	<.0001
AHA-3	83.6±19.9	261.4±70.8	178.4±49.3	130.1±31.9	99.6±23.6	80.8±18.4	68.4±15.8	59.1±14.4	<.0001
AHA-4	75.5±13.7	200.8±71.5	139.1±51.3	105.7±33.8	84.3±26.9	68.5±20.4	59.3±18.3	52.7±16.6	<.0001
AHA-5	78.3±14.7	178.2±76.2	127.7±47.0	95.7±31.0	75.8±21.5	63.8±15.4	55.9±13.5	49.9±11.6	<.0001
AHA-6	82.5±20.3	228.2±74.9	156.9±47.8	107.2±33.9	80.0±25.0	65.8±20.5	52.8±17.0	44.6±15.0	<.0001
AHA-7	75.5±11.0	187.5±75.2	136.0±49.3	96.5±34.0	74.4±24.4	61.5±20.1	54.4±17.5	48.4±15.4	<.0001
AHA-8	96.2±20.6	257.1±74.5	177.0±47.1	126.1±31.6	95.1±22.0	76.5±14.3	63.5±10.6	54.5±8.8	<.0001
AHA-9	86.6±19.8	262.3±85.0	178.7±59.8	132.6±36.7	101.9±26.0	83.3±20.5	71.6±17.7	62.7±16.2	<.0001
AHA-10	86.2±18.9	223.5±70.8	155.6±46.8	114.7±31.8	88.6±22.3	71.3±17.7	60.3±15.2	52.5±13.3	<.0001
AHA-11	86.4±14.6	237.5±81.1	164.7±52.4	119.6±34.2	91.1±24.4	74.3±20.1	63.7±18.4	55.6±16.8	<.0001
AHA-12	80.8±16.6	227.3±56.1	154.8±37.1	109.5±22.7	82.3±16.2	65.9±12.3	55.6±10.3	47.6±8.9	<.0001
AHA-13	68.4±13.8	197.6±67.0	139.4±44.2	101.9±31.6	78.7±23.1	64.1±16.0	55.2±12.8	48.7±11.1	<.0001
AHA-14	92.1±18.6	260.1±65.9	180.0±45.1	130.4±30.0	99.7±21.5	79.9±18.5	66.2±16.4	57.7±15.0	<.0001
AHA-15	75.6±19.2	214.3±66.9	151.7±43.0	111.3±26.5	86.2±17.2	71.6±13.0	61.9±10.8	54.6±9.2	<.0001
AHA-16	80.0±16.0	223.0±76.6	153.8±49.0	109.0±32.3	81.3±22.2	65.9±16.4	56.4±14.2	48.4±12.5	<.0001

Analysis of variance across energy levels. SE mean values are also depicted.

and at the anteroapical (50%) segments. Among the DE group, 17 (85%) patients showed at least one segment with BHA, most commonly located at the BIL (65%) and at the anteroapical segments (60%).

Among the DE group, the BIL segments showed significantly lower SD levels than most AHA myocardial segments (Table 5). The two segments most commonly affected by BHA (the BIL segment, AHA-5; and the anteroapical segment, AHA-13) [11] showed significantly lower SD levels at the lowest energy levels. These differences progressively diminished at higher energy levels and were undetected at 100 keV (Fig. 3).

Among the SE group, we did not find a significant relationship between BIL segment SD levels and body mass index ($r=0.05$, $P=.68$), heart rate ($r=-0.22$, $P=.35$), basal left ventricular chamber SD ($r=0.10$, $P=.67$), right ventricular chamber SD ($r=0.25$, $P=.29$), or descending aorta SD ($r=-0.09$, $P=.69$). Among the DE group, we did not find a significant relationship between the BIL SD levels and body mass index at any energy level (40 keV; $r=-0.36$, $P=.13$). Nevertheless, a significant relationship was found between BIL SD levels and descending aorta SD until 70 keV ($r=0.48$, $P=.04$), whereas at higher levels, no relationship was found (80 keV; $r=0.33$, $P=.17$; 90 keV; $r=0.30$, $P=.22$; 100 keV; $r=0.36$, $P=.12$). On the other hand, BIL SD levels at energy levels ≥ 70 keV were not significantly related to heart rate (70 keV; $r=0.07$, $P=.79$), basal left ventricular chamber SD (70 keV; $r=0.41$, $P=.08$), or right ventricular chamber SD (70 keV; $r=0.27$, $P=.26$).

9. Discussion

The main finding of our study was that BHA that influence the assessment of myocardial perfusion can be attenuated using DE imaging at increasing energy levels.

Several preclinical and clinical studies have validated the application of cardiac CT for the assessment of myocardial perfusion (CTP) using different scanners, pharmacological agents, and acquisition protocols [16,17]. CTP can be evaluated using two different approaches: static or dynamic CTP. Static CTP acquisitions, as used in our investigation, allow a qualitative assessment of CT attenuation-based myocardial perfusion evaluation based on myocardial SD levels, as well as the measurement of myocardial SD levels. Conversely, dynamic assessment of myocardial CTP provides quantitative estimation of myocardial time–attenuation curves and other parameters such as myocardial blood flow. Although there is a good agreement between methods and both have a high diagnostic performance for the detection of myocardial perfusion defects, dynamic CTP is associated to significantly higher radiation dose compared to static CTP [18,19].

Attenuation artifacts are considered an important limitation of CTP [20]. BHA are commonly observed in CTP studies and might resemble myocardial perfusion defects, affecting predominantly the BIL segment and less frequently other locations [11].

DE imaging appears as a promising technique towards CTP, driven by its ability to generate monochromatic image reconstructions that

Table 3
Myocardial SD ratio (defined as myocardial SD/left ventricular chamber SD) of left ventricular segments (AHA segmentation) among different energy levels using DE acquisitions

	SE	40 keV	50 keV	60 keV	70 keV	80 keV	90 keV	100 keV	*P* (ANOVA)
AHA-1	0.24±0.1	0.22±0.1	0.23±0.1	0.25±0.1	0.27±0.1	0.30±0.1	0.33±0.1	0.36±0.1	<.0001
AHA-2	0.27±0.1	0.29±0.1	0.30±0.1	0.32±0.1	0.34±0.1	0.36±0.1	0.38±0.1	0.40±0.1	.004
AHA-3	0.25±0.1	0.29±0.1	0.30±0.1	0.32±0.1	0.34±0.1	0.36±0.1	0.38±0.1	0.41±0.1	.001
AHA-4	0.23±0.1	0.22±0.1	0.23±0.1	0.25±0.1	0.28±0.1	0.30±0.1	0.33±0.1	0.36±0.1	<.0001
AHA-5	0.24±0.1	0.19±0.1	0.21±0.1	0.22±0.1	0.24±0.1	0.27±0.1	0.30±0.1	0.33±0.1	<.0001
AHA-6	0.25±0.1	0.25±0.1	0.26±0.1	0.26±0.1	0.26±0.1	0.29±0.1	0.30±0.1	0.30±0.1	.47
AHA-7	0.23±0.1	0.20±0.1	0.22±0.1	0.23±0.1	0.25±0.1	0.27±0.1	0.30±0.1	0.33±0.1	<.001
AHA-8	0.29±0.1	0.28±0.1	0.29±0.1	0.30±0.1	0.32±0.1	0.34±0.1	0.36±0.1	0.38±0.1	.055
AHA-9	0.26±0.1	0.28±0.1	0.29±0.1	0.31±0.1	0.32±0.1	0.36±0.1	0.40±0.1	0.43±0.1	<.0001
AHA-10	0.26±0.1	0.25±0.1	0.26±0.1	0.28±0.1	0.29±0.1	0.31±0.1	0.34±0.1	0.36±0.1	.003
AHA-11	0.26±0.1	0.26±0.1	0.27±0.1	0.28±0.1	0.30±0.1	0.32±0.1	0.35±0.1	0.37±0.1	.001
AHA-12	0.24±0.1	0.25±0.1	0.26±0.1	0.27±0.1	0.28±0.1	0.29±0.1	0.31±0.1	0.33±0.1	.068
AHA-13	0.21±0.1	0.22±0.1	0.24±0.1	0.25±0.1	0.26±0.1	0.29±0.1	0.31±0.1	0.34±0.1	.003
AHA-14	0.28±0.1	0.29±0.1	0.30±0.1	0.32±0.1	0.33±0.1	0.35±0.1	0.37±0.1	0.39±0.1	.03
AHA-15	0.23±0.1	0.24±0.1	0.25±0.1	0.27±0.1	0.29±0.1	0.32±0.1	0.35±0.1	0.38±0.1	<.0001
AHA-16	0.24±0.1	0.24±0.1	0.25±0.1	0.26±0.1	0.27±0.1	0.29±0.1	0.31±0.1	0.33±0.1	.006

Analysis of variance across energy levels. SE mean values are also depicted.

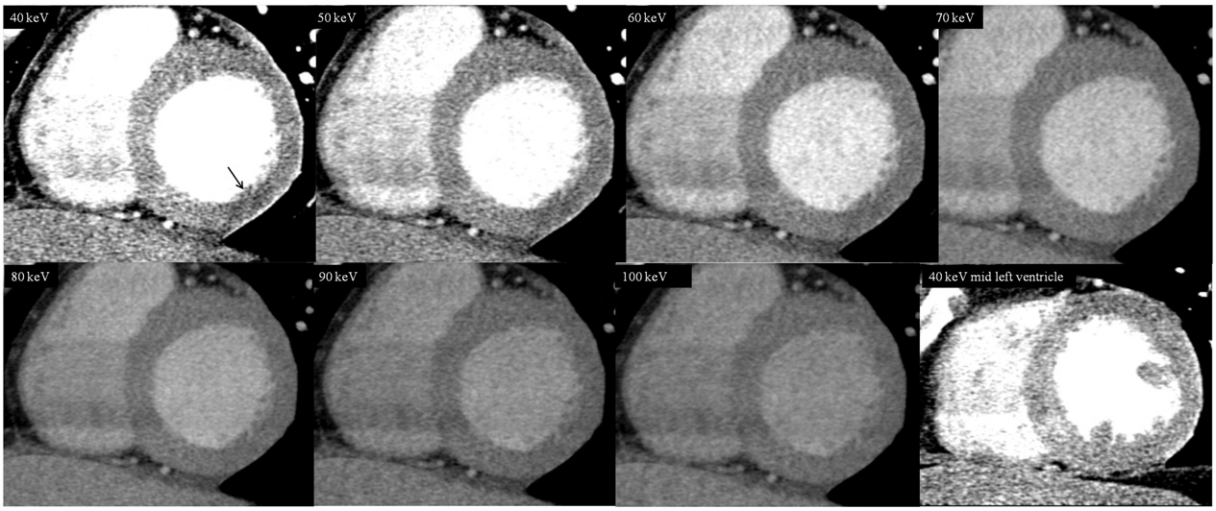

Fig. 1. Basal short-axis view using DE imaging at increasing energy levels from 40 to 100 keV. A significant drop in myocardial density is obvious at the lowest energy levels (arrow) with normal attenuation at the remaining segments, whereas at mid and higher energy levels, myocardial SD is homogeneous. The bottom right panel depicts the mid left ventricular segment at 40 keV, showing no BHA.

might improve some technical issues related to the polychromatic nature of X-rays.

10. Myocardial SD levels using DE imaging

One of the strengths of our study is the fact that we included nondiabetic patients with normal stress-rest myocardial perfusion and without evidence of CAD [21].

To the best of our knowledge, the present study is the first to establish the normal values of myocardial SD of left ventricular segments using DE imaging, as well as SD values normalized according to the left ventricular chamber SD (SD ratio). It is noteworthy that DE imaging was not related to an increase in effective dose radiation compared to SE imaging.

Acquaintance of these normal values is essential for the interpretation of CTP. As expected, among the DE group, myocardial SD levels were highest at low energy levels, with significantly lower SD levels at increasing energy levels. In turn, myocardial signal-to-noise ratio was not significantly influenced by the energy level applied given that the energy level is inversely related to both SD and noise [22]. Furthermore, in line with a previous study involving conventional SE imaging, mild regional differences regarding myocardial SD levels were observed and should therefore be accounted for in order to avoid misinterpretation of the results. It is noteworthy that CTP using DE imaging at the best energy level showed overall similar SD and signal-to-noise ratio levels compared to SE acquisitions among segments without BHA.

11. Attenuation of BHA with DE imaging

The BIL segment serves as a consistent location of BHA [11]. The selective filtration of low-energy photons by dense cardiac structures such as the descending aorta, the contrast-enhanced left ventricle, as well as bony structures such as the spine, sternum, and ribs, occasionally generates focal areas of nonphysiologic hypoenhancement within the myocardium. Given that all these highly attenuating structures are aligned along the same X-ray path as these myocardial segments, it is expected

Table 4
Myocardial signal-to-noise ratio of left ventricular segments (AHA segmentation) among different energy levels using DE acquisitions

	SE	40 keV	50 keV	60 keV	70 keV	80 keV	90 keV	100 keV	*P* (ANOVA)
AHA-1	4.3±1.4	3.2±1.6	3.2±1.4	3.7±1.7	3.7±1.6	4.0±1.6	3.4±1.3	3.3±1.2	.66
AHA-2	4.5±1.8	4.3±1.8	4.3±1.8	4.7±1.8	4.7±1.9*	5.0±1.9*	4.0±1.4	3.6±1.2	.28
AHA-3	4.2±2.0	4.4±1.8	4.3±1.9	4.9±1.8	4.9±1.8	5.1±1.9	4.3±1.7	4.0±1.5	.58
AHA-4	4.0±1.7	3.4±2.1	3.3±1.9	4.0±2.2	4.2±2.1	4.1±2.2	3.6±2.0	3.4±1.9	.68
AHA-5	5.1±2.4	2.8±1.3	2.9±1.3	3.4±1.4	3.8±1.5*	3.8±1.2*	3.4±1.2	3.3±1.2	.17
AHA-6	5.3±2.3	3.9±2.1	3.8±1.8	4.4±2.7	3.8±1.7	4.2±2.1	3.5±1.8	3.2±1.7	.63
AHA-7	5.5±2.4	3.3±1.9	3.4±1.6	3.8±1.7	3.8±1.5	3.9±1.8	3.5±1.7	3.5±1.6	.87
AHA-8	5.5±2.2	4.7±2.0	4.7±1.9	5.0±1.8	4.8±1.9	5.3±2.1	4.5±2.4	4.3±1.9	.85
AHA-9	5.1±3.0	4.5±2.4	4.6±2.5	5.3±2.7	5.3±2.5	5.9±3.2	4.8±2.5	4.7±2.3	.70
AHA-10	4.5±2.0	3.9±2.5	4.2±2.7	4.9±2.7	6.1±4.3‡	5.1±3.2	4.3±3.1	4.3±2.8	.31
AHA-11	6.7±3.2	4.7±3.2	4.8±3.7	5.5±4.5	5.9±4.1	5.2±3.3	4.2±2.5	4.4±2.6	.78
AHA-12	5.4±2.2	4.6±2.5	4.8±2.8	4.8±2.8	4.4±1.8	4.7±2.0	3.8±1.5	3.7±1.4	.56
AHA-13	4.4±1.9	3.7±1.8	3.8±1.8	4.1±1.7	4.2±1.7	4.1±1.7	3.8±1.8	3.6±1.6	.93
AHA-14	6.2±4.1	4.9±2.4	5.0±2.4	5.7±2.7	6.1±2.9†	5.6±2.6	4.4±1.7	4.5±1.7	.21
AHA-15	4.6±2.5	3.6±2.2	3.7±1.9	4.4±2.1	5.1±2.6†‡	4.3±1.7	3.7±1.3	3.7±1.6	.15
AHA-16	5.7±2.3	4.2±2.2	4.2±2.1	4.4±2.2	4.4±2.0	4.5±2.0	3.9±1.6	3.9±1.6	.90

Analysis of variance across energy levels. SE mean values are also depicted.
* $P<.05$ versus 100 keV (post hoc comparisons using LSD tests).
‡ $P<.05$ versus 40 and 50 keV (post hoc comparisons using LSD tests).
† $P<.05$ versus 90 and 100 keV (post hoc comparisons using LSD tests).

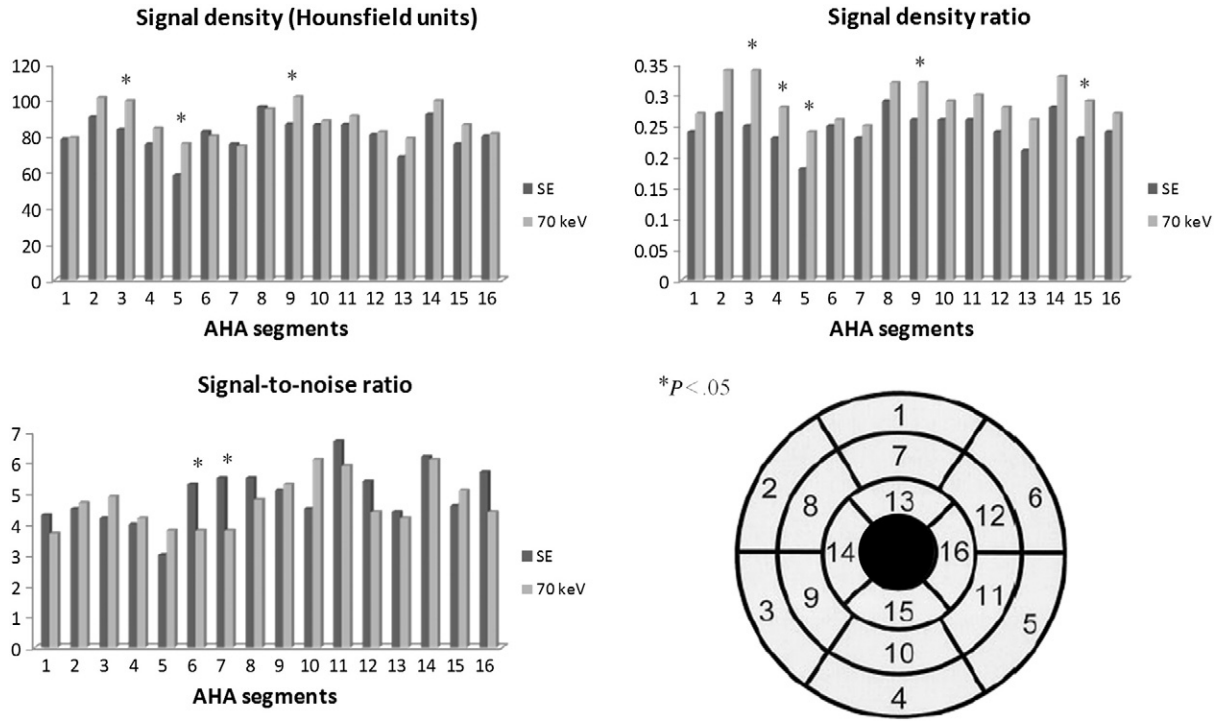

Fig. 2. Myocardial SD, SD ratio (defined as myocardial SD/left ventricular chamber SD), and signal-to-noise ratio of left ventricular segments (AHA segmentation) using SE and DE imaging at 70 keV.

that BHA are selectively observed in these segments. Indeed, both among the DE and the SE groups, the BIL segment showed significantly lower SD levels than most AHA myocardial segments. Finally, we demonstrated that using DE imaging, BHA observed at low energy levels diminish or even vanish at higher (≥90 keV) energy levels. It is worth mentioning that although BHA are considerably attenuated with increasing energy levels and this was clearly evident from visual analysis, cancellation of such artifacts is not fully guaranteed since myocardial SD levels at segments commonly influenced by BHA persist with a very mild decrease compared to some segments not affected by BHA. However, no significant differences are observed overall at or above 90 keV.

Our findings, although preliminary and hypothesis generating, might have relevant clinical implications regarding the interpretation of myocardial CTP since they provide energy thresholds at which discrimination between perfusion defects and BHA can be achieved. Future studies including larger populations as well as patients with perfusion deficits are warranted.

A number of limitations should be acknowledged. The relatively small sample size might lead to selection bias. Furthermore, image acquisition requires a number of heart beats, leading to potential nonuniform distribution of contrast in myocardial segments. Nonetheless, for that reason, blood SD at both left and right ventricles (at basal, mid,

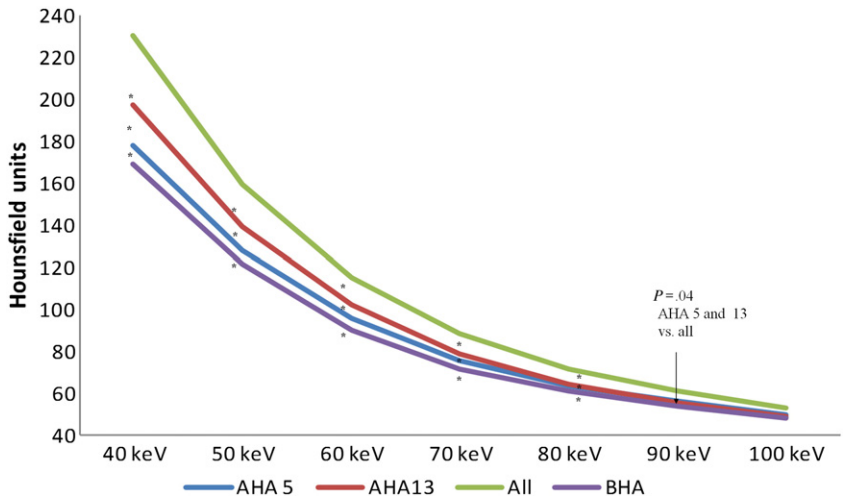

Fig. 3. Pairwise comparisons between myocardial SD levels at the same basal short-axis plane (BIL segment, AHA-5; and anteroapical segment, AHA-13 versus all myocardial segments). Only segments with BHA ($n=42$) are also plotted (independent-samples t test for comparison versus all myocardial segments). Significant differences (* denotes $P<.05$) are present among the lowest energy levels (40–60 keV), progressively declining at ≥70 keV. No differences are observed at the 100-keV energy level.

Table 5
Myocardial SD (HU): paired differences (*P* value) of left ventricular segments (AHA segmentation) versus the BIL segment (AHA-5) among different energy levels

	SE	40 keV	50 keV	60 keV	70 keV	80 keV	90 keV	100 keV
AHA-1	.99	.35	.47	.74	.75	.77	.73	.76
AHA-2	.04	<.0001	<.0001	<.0001	<.0001	<.0001	.002	.02
AHA-3	.29	<.0001	<.0001	<.0001	<.0001	<.0001	<.0001	<.0001
AHA-4	.44	.12	.24	.09	.09	.20	.37	.42
AHA-6	.40	.002	.002	.06	.26	.54	.43	.17
AHA-7	.45	.64	.41	.91	.81	.63	.77	.76
AHA-8	.003	<.0001	<.0001	<.0001	<.0001	.001	.02	.12
AHA-9	.05	.001	.003	<.0001	<.0001	<.0001	.001	.002
AHA-10	.09	.001	.002	.003	.007	.06	.27	.43
AHA-11	.02	.002	.002	.002	.004	.008	.03	.06
AHA-12	.50	.001	.002	.008	.03	.40	.91	.42
AHA-13	.01	.36	.43	.59	.81	.86	.69	.61
AHA-14	.03	<.0001	<.0001	<.0001	<.0001	<.0001	.002	.006
AHA-15	.54	.06	.05	.03	.03	.05	.14	.24
AHA-16	.74	.03	.04	.10	.34	.68	.97	.44

SE values are also depicted.

and apical levels) was obtained, and SD ratio enabled correction for potential nonuniform distribution of contrast.

12. Conclusions

In a nondiabetic population with normal myocardial perfusion and without evidence of CAD, BHA that influence the assessment of myocardial perfusion can be attenuated using DE imaging at increasing energy levels. Furthermore, myocardial perfusion evaluation using mid energy levels show similar SD and signal-to-noise ratio levels compared to SE acquisitions.

References

[1] Rodriguez-Granillo GA, Ingino CA, Lylyk P. Myocardial perfusion imaging and infarct characterization using multidetector cardiac computed tomography. World J Cardiol 2010;2:198–204.

[2] Ko SM, Choi JW, Song MG, Shin JK, Chee HK, Chung HW, et al. Myocardial perfusion imaging using adenosine-induced stress dual-energy computed tomography of the heart: comparison with cardiac magnetic resonance imaging and conventional coronary angiography. Eur Radiol 2011;21:26–35.

[3] Ko BS, Cameron JD, Leung M, Meredith IT, Leong DP, Antonis PR, et al. Combined CT coronary angiography and stress myocardial perfusion imaging for hemodynamically significant stenoses in patients with suspected coronary artery disease: a comparison with fractional flow reserve. JACC Cardiovasc imaging 2012;5:1097–111.

[4] Wang R, Yu W, Wang Y, He Y, Yang L, Bi T, et al. Incremental value of dual-energy CT to coronary CT angiography for the detection of significant coronary stenosis: comparison with quantitative coronary angiography and single photon emission computed tomography. Int J Cardiovasc Imaging 2011;27:647–56.

[5] Carrascosa PM, Deviggiano A, Capunay C, Campisi R, de Munain ML, Vallejos J, et al. Incremental value of myocardial perfusion over coronary angiography by spectral computed tomography in patients with intermediate to high likelihood of coronary artery disease. Eur J Radiol 2015;84(4):637–42.

[6] Meijboom WB, Van Mieghem CA, van Pelt N, Weustink A, Pugliese F, Mollet NR, et al. Comprehensive assessment of coronary artery stenoses: computed tomography coronary angiography versus conventional coronary angiography and correlation with fractional flow reserve in patients with stable angina. J Am Coll Cardiol 2008;52:636–43.

[7] Meijboom WB, van Mieghem CA, Mollet NR, Pugliese F, Weustink AC, van Pelt N, et al. 64-slice computed tomography coronary angiography in patients with high, intermediate, or low pretest probability of significant coronary artery disease. J Am Coll Cardiol 2007;50:1469–75.

[8] Gerber BL, Belge B, Legros GJ, Lim P, Poncelet A, Pasquet A, et al. Characterization of acute and chronic myocardial infarcts by multidetector computed tomography: comparison with contrast-enhanced magnetic resonance. Circulation 2006;113:823–33.

[9] Weininger M, Schoepf UJ, Ramachandra A, Fink C, Rowe GW, Costello P, et al. Adenosine-stress dynamic real-time myocardial perfusion CT and adenosine-stress first-pass dual-energy myocardial perfusion CT for the assessment of acute chest pain: initial results. Eur J Radiol 2012;81:3703–10.

[10] Kang DK, Schoepf UJ, Bastarrika G, Nance JW, Abro JA, Ruzsics B. Dual-energy computed tomography for integrative imaging of coronary artery disease: principles and clinical applications. Semin Ultrasound CT MR 2010;31:276–91.

[11] Rodriguez-Granillo GA, Rosales MA, Degrossi E, Rodriguez AE. Signal density of left ventricular myocardial segments and impact of beam hardening artifact: implications for myocardial perfusion assessment by multidetector CT coronary angiography. Int J Cardiovasc Imaging 2010;26:345–54.

[12] Carrascosa PM, Cury RC, Deviggiano A, Capunay C, Campisi R, Lopez de Munain M, et al. Comparison of myocardial perfusion evaluation with single versus dual-energy CT and effect of beam-hardening artifacts. Acad Radiol 2015. http://dx.doi.org/10.1016/j.acra.2014.12.019 [Epub ahead of print].

[13] Cerqueira MD, Weissman NJ, Dilsizian V, Jacobs AK, Kaul S, Laskey WK, et al. Registration for Cardiac I. Standardized myocardial segmentation and nomenclature for tomographic imaging of the heart. A statement for healthcare professionals from the Cardiac Imaging Committee of the Council on Clinical Cardiology of the American Heart Association. Int J Cardiovasc Imaging 2002;18:539–42.

[14] George RT, Silva C, Cordeiro MA, DiPaula A, Thompson DR, McCarthy WF, et al. Multidetector computed tomography myocardial perfusion imaging during adenosine stress. J Am Coll Cardiol 2006;48:153–60.

[15] Gibbons RJ, Balady GJ, Bricker JT, Chaitman BR, Fletcher GF, Froelicher VF, et al. American College of Cardiology/American Heart Association Task Force on Practice Guidelines. Committee to Update the Exercise Testing G. ACC/AHA 2002 guideline update for exercise testing: summary article. A report of the American College of Cardiology/American Heart Association Task Force on Practice Guidelines (Committee to Update the 1997 Exercise Testing Guidelines). J Am Coll Cardiol 2002;40:1531–40.

[16] Blankstein R, Shturman LD, Rogers IS, Rocha-Filho JA, Okada DR, Sarwar A, et al. Adenosine-induced stress myocardial perfusion imaging using dual-source cardiac computed tomography. J Am Coll Cardiol 2009;54:1072–84.

[17] Hoffmann U, Millea R, Enzweiler C, Ferencik M, Gulick S, Titus J, et al. Acute myocardial infarction: contrast-enhanced multi-detector row CT in a porcine model. Radiology 2004;231:697–701.

[18] Kurata A, Kawaguchi N, Kido T, Inoue K, Suzuki J, Ogimoto A, et al. Qualitative and quantitative assessment of adenosine triphosphate stress whole-heart dynamic myocardial perfusion imaging using 256-slice computed tomography. PLoS One 2013;8:e83950.

[19] Rossi A, Merkus D, Klotz E, Mollet N, de Feyter PJ, Krestin GP. Stress myocardial perfusion: imaging with multidetector CT. Radiology 2014;270:25–46.

[20] Schwitter J, Wacker CM, van Rossum AC, Lombardi M, Al-Saadi N, Ahlstrom H, et al. MR-impact: comparison of perfusion-cardiac magnetic resonance with single-photon emission computed tomography for the detection of coronary artery disease in a multicentre, multivendor, randomized trial. Eur Heart J 2008;29:480–9.

[21] Scheske JA, O'Brien JM, Earls JP, Min JK, LaBounty TM, Cury RC, et al. Coronary artery imaging with single-source rapid kilovolt peak-switching dual-energy CT. Radiology 2013;268:702–9.

[22] Carrascosa P, Capunay C, Rodriguez-Granillo GA, Deviggiano A, Vallejos J, Leipsic JA. Substantial iodine volume load reduction in CT angiography with dual-energy imaging: insights from a pilot randomized study. Int J Cardiovasc Imaging 2014;30(8):1613–20.